J Solid State Electrochem (2011) 15:2683–2693
DOI 10.1007/s10008-010-1259-6

ORIGINAL PAPER

A study of the electrochemical behavior of an oxadiazole derivative electrodeposited on multi-wall carbon nanotube-modified electrode and its application as a hydrazine sensor

Navid Nasirizadeh · Hamid R. Zare · Ali R. Fakhari · Hamid Ahmar · Mohammad R. Ahmadzadeh · Amin Naeimi

Received: 22 September 2010 / Revised: 19 November 2010 / Accepted: 23 November 2010 / Published online: 15 December 2010

Abstract In this study, an oxadiazole multi-wall carbon nanotube-modified glassy carbon electrode (OMWCNT−GCE) was used as a highly sensitive electrochemical sensor for hydrazine determination. The surface charge transfer rate constant, k_s, and the charge transfer coefficient, α, for electron transfer between GCE and electrodeposited oxadiazole were calculated as 19.4±0.5 s^{-1} and 0.51, respectively at pH=7.0. The obtained results indicate that hydrazine peak potential at OMWCNT−GCE shifted for 14, 109, and 136 mV to negative values as compared with oxadiazole-modified GCE, MWCNT−GCE, and activated GCE surface, respectively. The electron transfer coefficient, α, and the heterogeneous rate constant, k', for the oxidation of hydrazine at OMWCNT−GCE were also determined by cyclic voltammetry measurements. Two linear dynamic ranges of 0.6 to 10.0 μM and 10.0 to 400.0 μM and detection limit of 0.17 μM for hydrazine determination were evaluated using differential pulse voltammetry. In addition, OMWCNT−GCE was shown to be successfully applied to determine hydrazine in various water samples.

Keywords Oxadiazole · Hydrazine · Electrocatalytic oxidation · Multi-wall carbon nanotubes

N. Nasirizadeh (✉) · M. R. Ahmadzadeh
Department of Chemistry, Islamic Azad University,
Yazd Branch,
Yazd, Iran
e-mail: nasirizadeh@yahoo.com

H. R. Zare
Department of Chemistry, Yazd University,
P.O. Box 89195-741, Yazd, Iran

A. R. Fakhari · H. Ahmar
Department of Chemistry, Shahid Beheshti University,
Tehran, Iran

A. Naeimi
Young Researchers Club, Islamic Azad University,
Khatam Branch,
Yazd, Iran

Introduction

Hydrazine is a compound of interest in both chemical and pharmaceutical industry because it is a reagent for the preparation of several pharmaceutical derivatives [1–4]. It is also a strong reducing agent used as oxygen scavenger for corrosion control in boilers and hot water heating systems [5]. Hydrazine is used in agriculture as pesticide, pharmaceutical intermediate, photographic chemical, corrosion inhibitor, antioxidant, catalyst, emulsifier, and reducing agent [6]. Despite the wide use of hydrazine in various areas, it has been known to be harmful for human life. Hydrazine is volatile, toxic, and readily absorbed by oral, dermal, or inhalation routes of exposure. Acute exposure can also damage the liver, the kidneys, and the central nervous system [7, 8]. Due to the environmental and toxicological significance of hydrazine compounds, the development of sensitive and selective analytical methods for the determination of hydrazine is necessary. Different

methods have been proposed for the determination of hydrazine such as spectrophotometric [9–12], chemiluminescence [13, 14], fluorescence [15], and electrochemical methods [16, 17].

Among these, electroanalytical techniques have been proven to be relatively direct and effective for the detection of hydrazine and its derivatives [18]. Nevertheless, direct oxidation of hydrazine has been limited by a substantial overpotential at conventional carbon electrodes. Besides, ordinary carbon electrodes have a low sensitivity and also a reproducibility, and slow electron transfer. One promising approach for lowering overpotential to facilitate the determination is via the electrocatalytic process at chemically modified electrodes [19]. Compounds which improve anodic oxidation of hydrazine are chlorogenic acid [20, 21], rutin [22], caffeic acid [23], pyrocatechol violet [24], hematoxyline [25], coumestan derivative [26], and catechin [27].

Carbon nanotube (CNT) electrodes have recently drawn great attention in electrochemical research owing to their low electrical resistance, high accessible surface area, chemical stability, and enhanced sensing properties [28, 29]. CNTs are adsorbed on the surface of the electrode and comprise a three-dimensional and porous network. As shown in the SEM photograph of some previous studies, the stem-like structure of the coating confirmed the presence of CNTs on GCE surface [30, 31]. The unique structure of carbon nanotubes makes it possible for them to be used as a new support for catalysts [32, 33]. These properties of CNTs have been used to promote the electron transfer reaction for a wide range of molecules and biological species, especially when applied as electrode materials in electrochemical devices [34, 35]. In most reports, deposited modifiers on CNT-modified electrodes were used for the electrocatalytic determination of the various analytes [36, 37]. In this study, the preparation of an oxadiazole derivative multi-wall carbon nanotube-modified glassy carbon electrode (OMWCNT−GCE) and its application for the electrocatalytic oxidation of hydrazine are reported.

Experimental

Chemicals

An oxadiazole derivative, 4-(5-phenyl-1, 3, 4-oxadiazole-2-thiol)-5-methylbenzen-1,2-diol, (see Scheme 1 for the structure) was synthesized, purified, and characterized according to the procedure described before [38]. In the present paper, we refer to this derivative as oxadiazole for convenience. Hydrazine and dimethyl formamide (DMF) were purchased from Merck and used as received. The multi-wall carbon nanotubes (>95% purity, 10–20 nm diameter, 5–20 μm length) were obtained from Nanolab Inc. (Brighton, MA, USA). The immobilizing solution of MWCNT was prepared by introducing 5 mg of MWCNT into 5 ml of DMF. All other solutions were prepared with twice-distilled water. The buffer solution (0.1 M) was made up of H_3PO_4+NaH_2PO_4, and the pH was adjusted by using 0.1 M H_3PO_4 and 2.0 M NaOH.

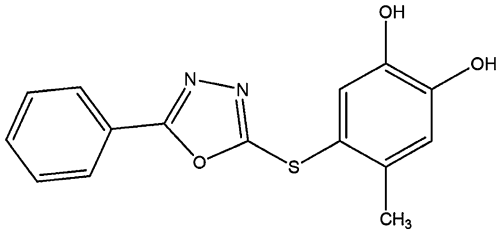

Scheme 1 Structure of oxadiazole derivative

Instrument and procedures

Electrochemical measurements were performed with an Autolab potentiostat/galvanostat Type III (Eco chemic Utrecht, Netherlands) and GPES 4.9 software of at laboratory temperature (25±1 °C). A three-electrode electrochemical cell was employed for all electrochemical measurements. The working, counter, and reference electrodes were oxadiazole multi-wall carbon nanotube-modified glassy carbon electrode, platinum electrode and Ag/AgCl (sat.), KCl (3 M), respectively. The differential pulse voltammetry (DPV) was used with an amplitude of 25 mV, a modulation time 0.05 s and a step potential of 50 mV in the 0.1 M phosphate buffer solution (pH 7.0) and scanning the electrode potential between 0.03 and 0.22 V. All potentials in the text were reported with respect to this reference electrode. The pH measurements were done using a Metrohm model 827 pH/mV meter.

Preparation of oxadiazole-modified GCE, MWCNT-modified GCE, and OMWCNT-modified GCE

Prior to the modification, GCE was carefully polished mechanically with 0.05 μm Al_2O_3 slurry on the polishing cloth and then rinsed with doubly distilled water. After being cleaned, for electrochemical activation of the electrode, it was immersed in a 0.1 M sodium bicarbonate solution and was activated by a continuous potential cycling from −1.45 to 1.75 V at a sweep rate of 100 mV s^{-1}, until a stable voltammogram was obtained. For the preparation of oxadiazole-modified GCE (OMGCE), the activated GCE (AGCE) was rinsed with doubly distilled water and was modified by ten cycles of potential sweep between −180 and 580 mV at 50 mV s^{-1} in 0.2 mM solution of oxadiazole in 0.1 M phosphate buffer (pH 7.0). The fabrication of the MWCNT and the

OMWCNT−GCE is described as follows. A 3 μl of MWCNT−DMF solution (1.0 mg ml^{-1}) was placed directly onto a GCE surface and dried at room temperature to form a MWCNT film at a GCE surface and preparation of the MWCNT-modified GCE (MWCNT−GCE). The effective surface area of the MWCNT−GCE was estimated from the cyclic voltammograms of 1.0 mM $K_3[Fe(CN)_6]$ solution at various scan rates. For a reversible process, the Randles-Sevcik formula was used [39].

$$I_{pa} = 2.69 \times 10^5 n^{3/2} A C_O D_R^{1/2} v^{1/2} \quad (1)$$

where I_{pa} refers to the anodic peak current, n the number of electrons transferred, A the surface area of the electrode, D the diffusion coefficient, C_O the concentration of $K_3[Fe(CN)_6]$, and ν is the scan rate. For 1.0 mM $K_3[Fe(CN)_6]$ in the 0.1 M KNO_3 electrolyte: $n=1$ and $D = 7.6 \times 10^{-6} cm^2 s^{-1}$ [39], then from the slope of the I_{pa} versus $v^{1/2}$, the effective areas were calculated as 0.03 cm^2. The OMWCNT−GCE was prepared by immersing the MWCNT−GCE in a 0.2 mM solution of oxadiazole in 0.1 M phosphate buffer (pH 7.0) and using ten cycles of potential sweep between −180 and 580 mV at 50 mV s^{-1} (Fig. 1, inset A). After the formation of oxadiazole film on

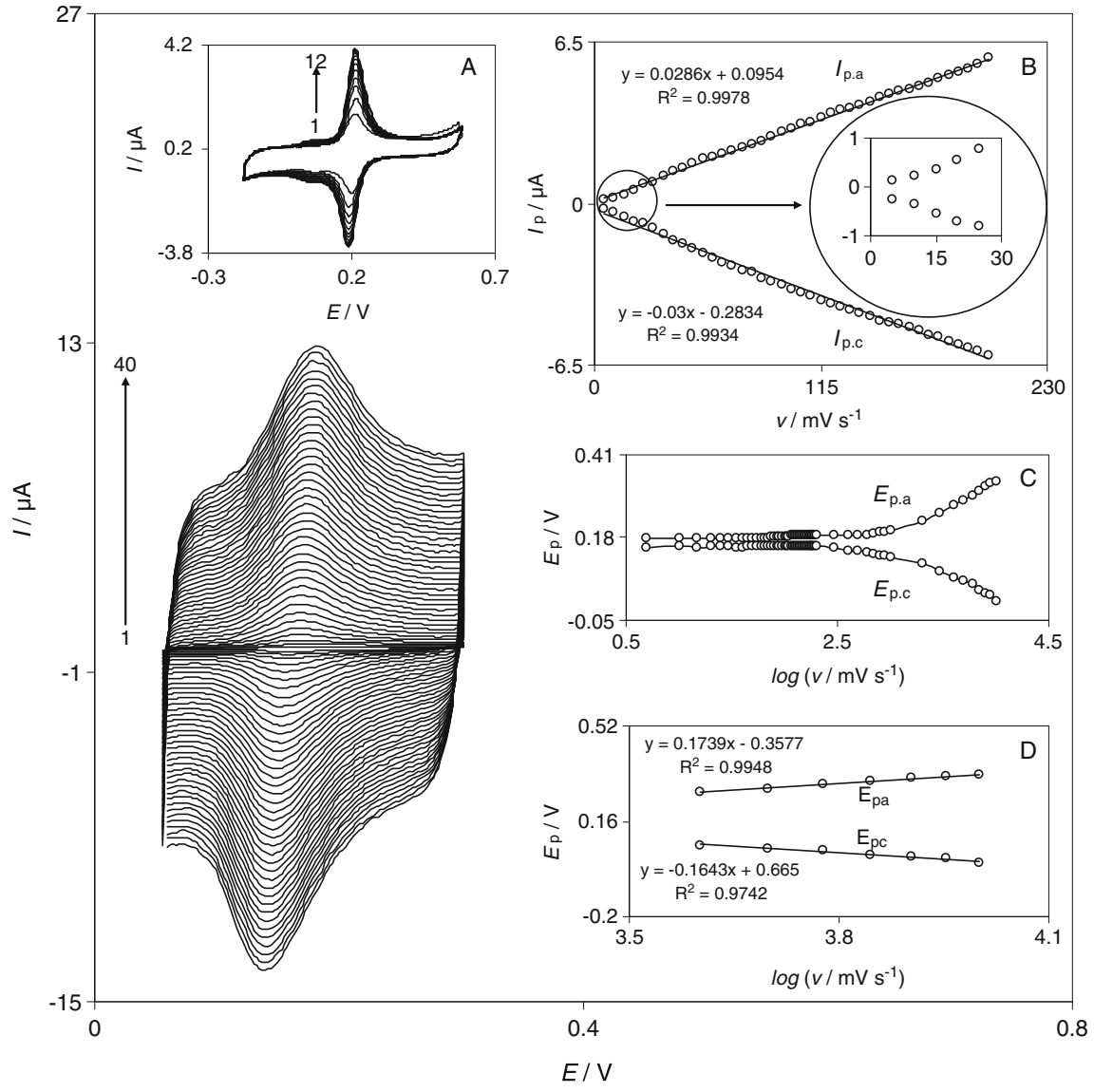

Fig. 1 Cyclic voltammetric responses of OMWCNT−GCE in 0.1 M phosphate buffer (pH 7.0) at different scan rates (5–200 mV s^{-1}). *Insets*: *A* cyclic voltammograms of a 0.2 mM oxadiazole solution at AGCE in 0.1 M phosphate buffer solution (pH 7.0) at scan rate 50 mV s^{-1}. The number of *1–12* corresponds to the sweep number of potential cycles during the modification step. *B* Plots of anodic and cathodic peak currents vs. of scan rate. *C* Variation of the peak potentials vs. the logarithm of the scan rate. *D* Magnification of the same plot for high scan rates

MWCNT−GCE surface, the modified electrode was rinsed thoroughly with water and was dipped into the buffer solution to test its electrochemical behavior.

Results and discussion

Electrochemistry behavior of OMWCNT-modified GCE

In recent years, reports regarding the electrodeposition mechanism of *o*-hydroquinone derivatives onto an electrode surface have been published [40–42]. The electrodeposition mechanism of these compounds was explained on the basis of the nucleophilic attack of functional groups of the electrode surface against the *o*-quinone ring which formed from oxidation of the *o*-hydroquinone moiety of the modifier [40], formation of a polymer layer on the electrode surface [41], or adsorption of the modifier at the electrode surface [42]. For the nucleophilic attack or polymer formation, it is necessary that one of the positions 4 or 5 of *o*-quinone ring of modifier is unoccupied. Since the positions 4 and 5 of the *o*-hydroquinone ring of the oxadiazole derivative are occupied, it is rational to conclude that the deposition mechanism of oxadiazole is based on its adsorption at the electrode surface.

Figure 1 shows the cyclic voltammograms of the OMWCNT−GCE in 0.1 M phosphate buffer solution (pH 7.0) at various potential scan rates. The plots of the anodic and cathodic peak currents versus the scan rate exhibit a linear relation (Fig. 1, inset B) as predicted theoretically for a surface-immobilized redox couple. Further, the ratio of I_{pa}/I_{pc} was found to be almost constant in the studied range. Moreover, because of the facility of charge transfer kinetics over the range of 5 to 1,000 mV s^{-1}, the formal potential, $E^{0\prime}$, was almost independent of the potential scan rate for sweep rates at this range. The peak-to-peak potential separation (ΔE_p) was rather low, ca. 48 mV for the sweep rates below 2,000 mV s^{-1}. According to the method described by Laviron [43], the electron transfer coefficient, α, as well as the heterogeneous rate constant, k_s, for the charge transfer between the electrode and the surface confined redox couple can be calculated from the slope of variation of E_p versus log *v*. Figure 1, insets C and D, show that the values of the anodic and cathodic peak potentials were proportional to the logarithm of scan rate for scan rates higher than 4,000 mV s^{-1}. Using the slope of plots in Fig. 1, inset D, the values of α=0.51 and $k_s = 19.4 \pm 0.5\ s^{-1}$ were obtained at pH 7.0. This k_s value is greater than these previously reported for modifiers of pyrocatechol violet (k_s=5.3 s^{-1}) [24], catechin (k_s=3.77 s^{-1}) [27], and tetrabromo-*p*-benzoquinone (k_s=3.8 s^{-1}) [44]. The high electron transfer rate constant makes our oxidiazole derivative an excellent electron transfer mediator for electrocatalytic processes. It is to be noted that the scan rate inevitably induces the increase of the ohmic drop which, in turn, makes the shift of peak potential in larger value dependent on the ohmic drop as well as the slow kinetic electron transfer. In this respect, there appears to be an unavoidable error in the k_s value computation. Also, there are different errors in the reported k_s values of various deposited modifiers, because the error values dependent on the ohmic drop values of the used systems.

In the present case, the values of α and k_s were pH dependent. The values of α and k_s were obtained at four pH and the results are summarized in Table 1.

Since oxadiazole has an *o*-quinone moiety, it was anticipated that the redox response of the oxadiazole film would be pH dependent. Therefore, the cyclic voltammetric responses of an OMWCNT−GCE were obtained in buffered solutions of various pH from 2 to 10 (Fig. 2a). As shown in Fig. 2b, the formal potential, $E^{0\prime} = E_{p.a} - a\left(E_{p.a} - E_{p.c}\right)$ [45], shifted to the less positive potential with the increasing of the solution pH value, indicates that proton participates in the redox reaction of oxadiazole. The slope of the variation of $E^{0\prime}$ as a function of solution pH (0.058 V/pH unit) is close to the Nernstian slope of 0.059 VpH^{-1} unit at 25 °C and indicates that the number of electrons and protons involved in the electrode process is equal. The redox reactions in oxadiazole aqueous solution as one of ortho-quinon derivatives occur with the participation of two electrons. Hence there are two protons transferred in the redox reaction in the pH range of 2.0–10.0.

Electrocatalytic oxidation of hydrazine at an OMWCNT-modified GCE

In order to evaluate the electrocatalytic activity of the oxadiazole film electrodeposited on GCE toward the oxidation of hydrazine, cyclic voltammograms of bare GCE (BGCE), AGCE, OMGCE, MWCNT−GCE, and OMWCNT−GCE were obtained in the absence and presence of 0.2 mM hydrazine (Fig. 3). In the absence of hydrazine, a pair of well-defined redox peaks of OMGCE (curve a) and OMWCNT−GCE (curve c) can be observed. Upon the addition of 0.2 mM hydrazine, there is a drastic enhancement of the anodic peak current, and no cathodic current was observed in the reverse scan for the both

Table 1 The surface charge transfer rate constant, k_s, and the charge transfer coefficient, α, for the electron transfer between MWCNT–GCE and the oxadiazole at various pH

pH	α	k_s/s^{-1}
3	0.51	3.5±0.09
5	0.52	4.6±0.1
7	0.51	19.4±0.5
9	0.55	17.7±0.5

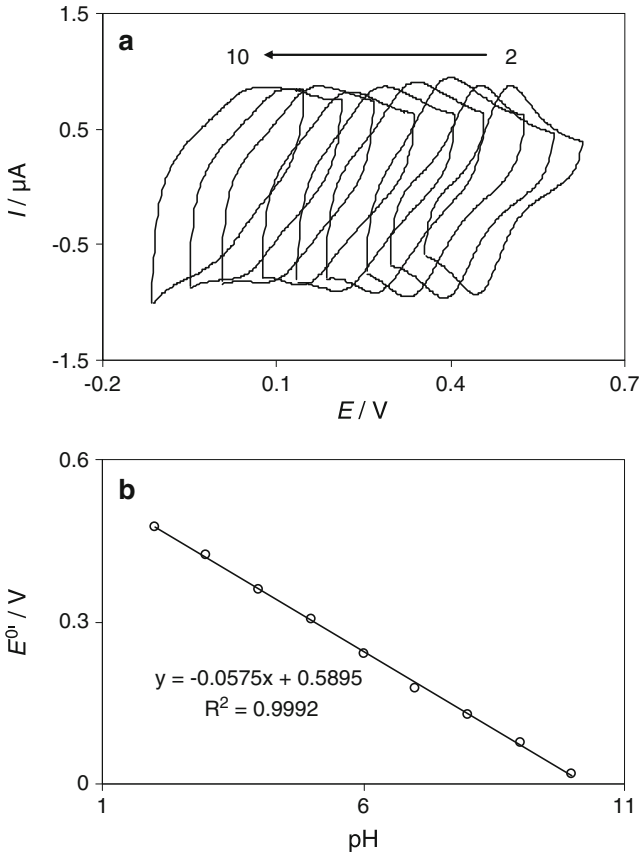

Fig. 2 **a** Cyclic voltammograms (at 50 mV s^{-1}) for OMWCNT−GCE in buffered pHs of 2.0, 3.0, 4.0, 5.0, 6.0, 7.0, 8.0, 9.0, and 10.0, respectively. **b** Plot of the formal potential, $E^{0\prime}$, vs. pH

modified electrodes (Fig. 3, curves b and d). This behavior is consistent with a very strong electrocatalytic effect [20–27, 46]. To approve the electrocatalytic effect, the dependence of the voltammetric response of OMGCE on hydrazine concentration in pH=7.0 is shown in inset of Fig. 3. As it is shown, the anodic peak current increased and the cathodic peak current decreased with increasing of the hydrazine concentration which it indicates the electrocatalytic oxidation of hydrazine at OMGCE. According to the catalytic current responses of voltammograms b and d, there is a dramatic enhancement of the anodic peak current at OMWCNT–GCE (voltammograms d) in relation to the value obtained at the OMGCE. In fact, the higher current responses of OMWCNT–GCE or MWCNT as compared to other modified electrodes (OMGCE or AGCE) are due to the increase of the surface area of OMWCNT–GCE and MWCNT–GCE. Also, the peak potential of hydrazine oxidation at OMWCNT−GCE (curve d) shifted by about 14, 109, and 156 mV to more negative values compared with the OMGCE (curve b), MWCNT−GCE (curve e), and AGCE (curve f), respectively. Comparison of curves f and b shows that the current response of hydrazine oxidation at AGCE is higher than at OMGCE. Indeed, during the modification of AGCE by oxadiazole modifier, some of its active sites (no all of its active sites) occupied by oxadiazole molecules. Thus, it is rationalized the current response of hydrazine oxidation at the OMGCE surface which appears at less positive potential (E_p=270 mV) decreases as compared with the current response at AGCE

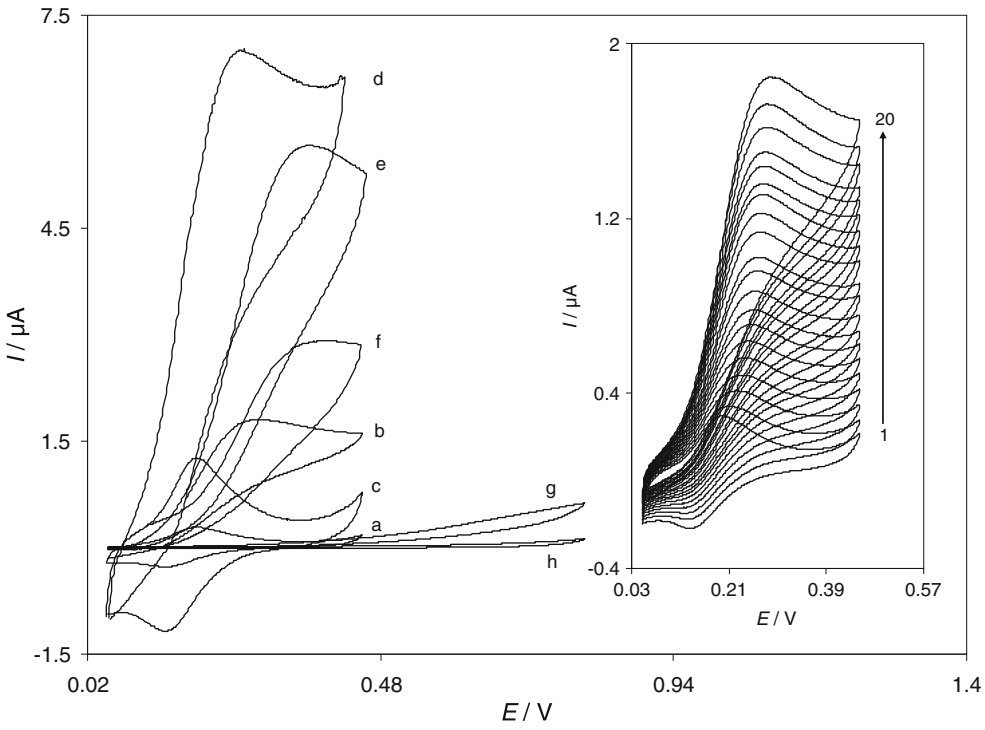

Fig. 3 Cyclic voltammograms of an OMWCNT−GCE in 0.1 M phosphate buffer solution (pH 7.0) at scan rate 20 mV s^{-1} in the absence (*c*) and presence of 0.2 mM hydrazine (*d*). *a* as *c* and *b* as *d* for an oxadiazole-modified GCE. *e*, *f*, and *g* as *d* and *h* as *c* for MWCNT−GCE, AGCE, and BGCE. *Inset*: cyclic voltammograms of an OMGCE in 0.1 M phosphate buffer solution containing various concentrations of hydrazine at 20 mV s^{-1}. The number of 1−20 correspond to different concentrations of 0.0–0.2 mM of hydrazine

Table 2 Comparison of electrocatalytic oxidation of hydrazine (0.5 mM) on various electrode surfaces at pH 7.0

Name of electrode	Oxidation potential (mV)	Oxidation current (μA)
OMGCE	270	1.2
AGCE	392	2.0
MWCNT−GCE	365	3.4
OMWCNT−GCE	256	3.8

OMGCE oxadiazole-modified glassy carbon electrode, *AGCE* activated glassy carbon electrode, *MWCNT−GCE* multi-wall carbon nanotube-modified glassy carbon electrode, *OMWCNT−GCE* oxadiazole/multi-wall carbon nanotube-modified glassy carbon electrode

surface (E_p=392 mV). When the hydrazine oxidation at AGCE (curve f) and MWCNT−GCE (curve e) surfaces were compared, it was observed that the current of hydrazine oxidation increased and the peak potential was shifted to lower values in the presence of MWCNT. This is probably due to the MWCNT dimensions (of the tubes, the channels that are inherently present in the tubes), the electronic structure, and the topological defects present on the tube surface [47]. Also, as it can be seen, at BGCE no current is observed in the presence of hydrazine (voltammogram g). The electrocatalytic oxidation characteristics of hydrazine at various modified electrode surfaces at pH 7.0 are summarized in Table 2. This stands to the fact that the electrooxidation of hydrazine is greatly improved at OMWCNT−GCE. Therefore, MWCNT can be used as a new material for immobilization and electron transfer reactions of oxadiazole.

Figure 4a shows the cyclic voltammograms of the OMWCNT−GCE at various scan rates obtained in 0.1 M phosphate buffer solution (pH 7.0) containing 0.2 mM hydrazine. The peak current for the anodic oxidation of hydrazine is proportional to the square root of scan rate (inset of Fig. 4a). The results also indicate that at a potential higher than the peak potential the reaction

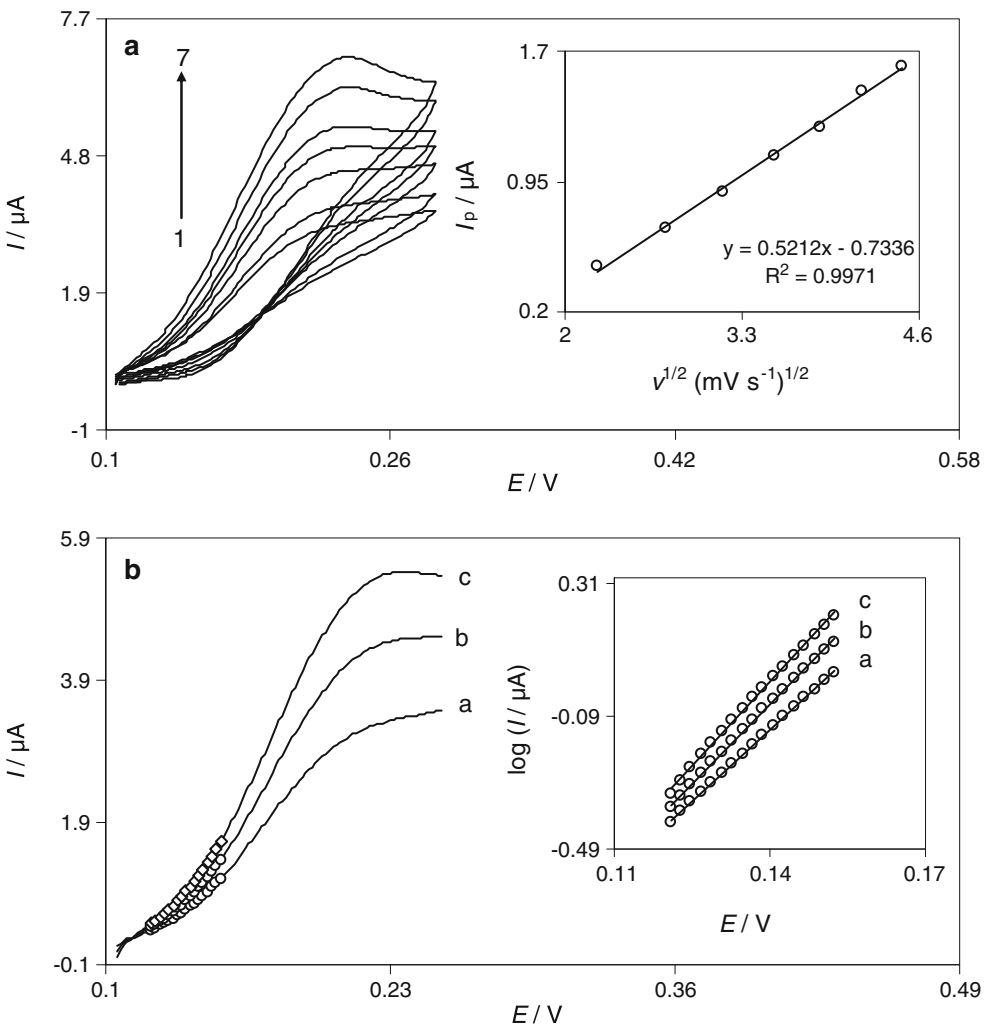

Fig. 4 **a** Cyclic voltammograms of an OMWCNT−GCE in 0.1 M phosphate buffer solution (pH 7.0) containing 0.2 mM hydrazine. The numbers *1–7* correspond to scan rates of 5.0, 7.5, 10.0, 12.5, 15.0, 17.5, and 20.0 mV s^{-1}. *Inset* shows the variation of the electrocatalytic peak current vs. the square root of scan rate. **b** Linear sweep voltammograms of OMWCNT−GCE in 0.1 M phosphate buffer (pH 7.0) containing 0.2 mM hydrazine at scan rates of *a* 5 mV s^{-1}, *b* 10 mV s^{-1}, and *c* 15 mV s^{-1}. The points are the data used in the Tafel plots. *Inset* shows the Tafel plots derived from linear sweep voltammograms

involves mass transport. Under this condition the peak current depends on hydrazine concentration, which is an ideal case for quantitative applications. According to the following equation for a totally irreversible diffusion controlled process [48],

$$I_p = 3.01 \times 10^5 n[(1-a)na]^{1/2} A C_b D^{1/2} v^{1/2} \quad (2)$$

and considering $(1-\alpha)n\alpha=0.8$ (see below), $D = 6.6 \times 10^{-6}\text{cm}^2\,\text{s}^{-1}$ (D was determined by chronoamperometry), and $A=0.03$ cm^2, it is estimated that the total number of electrons involved in the anodic oxidation of hydrazine is $n = 3.8 \cong 4$. Thus, based on this result, the catalytic mechanism can be expressed as shown in following scheme:

$$\text{Oxadiazole} \underset{}{\overset{k_s}{\rightleftharpoons}} \text{Oxadiazole}_{(ox)} + 2e^- + 2H^+ \qquad (E_r) \qquad (3)$$

$$2\text{Oxadiazole}_{(ox)} + N_2H_4 \xrightarrow{k'_h} 2\text{Oxadiazole} + N_2 \qquad (C'_i) \qquad (4)$$

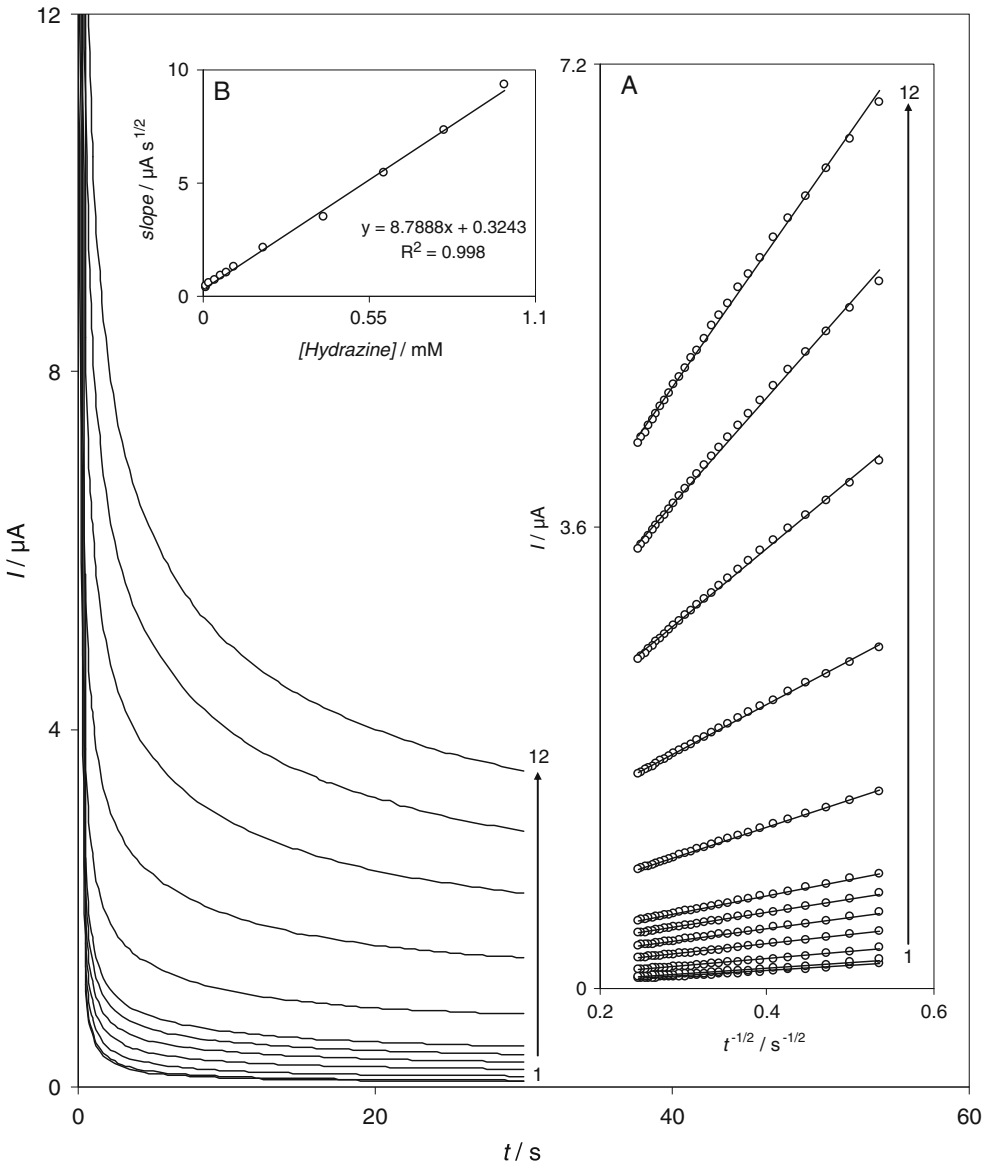

Fig. 5 Chronoamperometric response at an OMWCNT–GCE in 0.1 M phosphate buffer (pH 7.0) at a potential step of 260 mV for different concentrations of hydrazine. The numbers *1–12* correspond to 8.0, 10.0, 20.0, 40.0, 60.0, 80.0, 100.0, 200.0, 400.0, 600.0, 800.0, and 1,000.0 µM of hydrazine. *Insets*: *A* plots of I vs. $t^{-1/2}$ obtained from the chronoamperograms and *B* plot of the slope of the straight lines against the hydrazine concentration

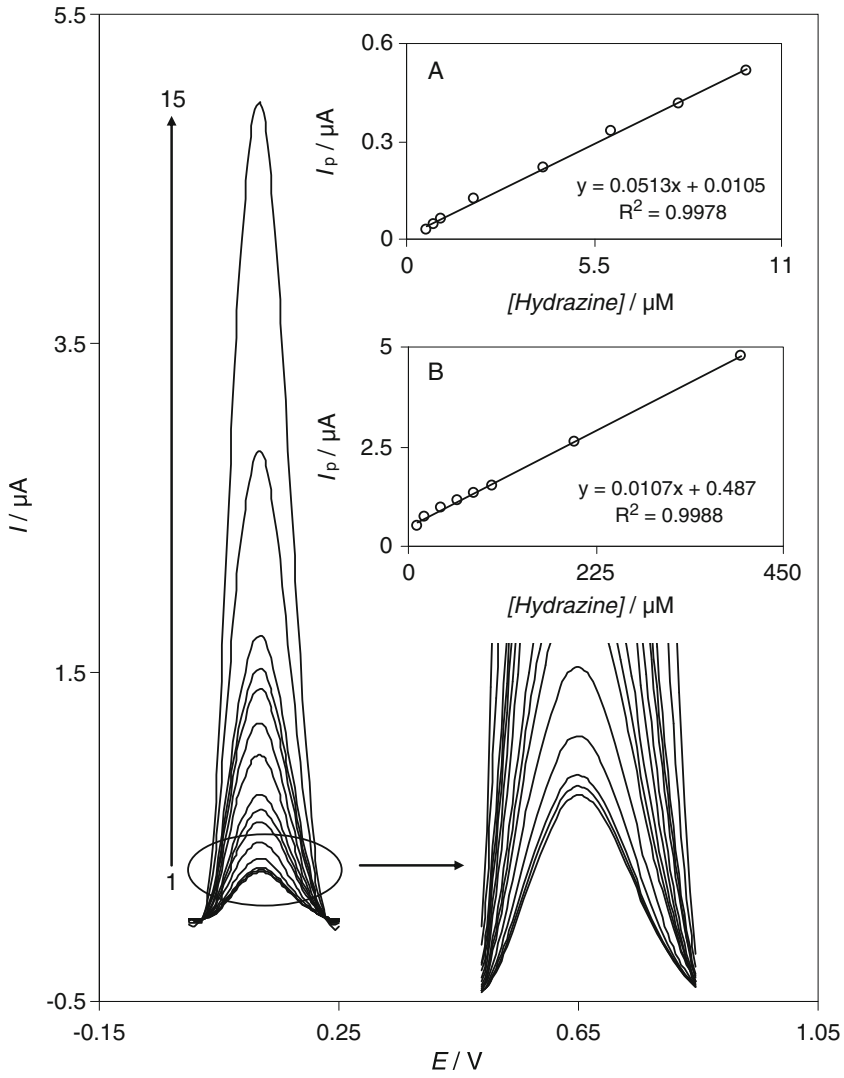

Fig. 6 Differential pulse voltammograms of an OMWCNT–GCE in 0.1 M phosphate buffer solution (pH 7.0) containing different concentrations of hydrazine. The numbers of *1–15* correspond to 0.6, 0.8, 1.0, 2.0, 4.0, 6.0, 8.0, 10.0, 20.0, 40.0, 60.0, 80.0, 100.0, 200.0, and 400.0 μM hydrazine. *Insets* show the plots of the electrocatalytic peak current, corrected for any residual current, as a function of hydrazine concentration in the range of *A* 0.6–10.0 μM and *B* 10.0–400.0 μM

Andrieux and Saveant theoretical model [49] can be used to calculate the catalytic rate constant between hydrazine and oxadiazole, k'. According to the theoretical model of Andrieux and Saveant and using Fig. 4 in their theoretical paper [49], the average value of k' was calculated to be $(2.8\pm0.06)\times10^{-3}$ cm s^{-1}.

Table 3 Comparison of some of the analytical characteristics for hydrazine determination in non-electrochemical techniques and those obtained in the present study

Method	Linear range (μM)	Detection limit (μM)	Reference
Spectophotometric	0.3–32.0	0.08	[10]
Spectophotometric	0–21.9	0.7	[11]
Spectophotometric	0.6–15.6	0.3	[12]
Spectophotometric	4.7–31.0	3.1	[13]
Chemiluminescence	0.5–100.0	0.2	[14]
Fluorescence	0.2–9.3	0.08	[15]
DPV	0.6–10.0 10.0–400.0	0.17	This work

Figure 4b shows the anodic linear sweep voltammograms recorded at 5.0, 10.0, and 15.0 mV s^{-1}. The points shown are from the rising part of the voltammograms which corresponds to Tafel behavior as affected by electron transfer kinetics between hydrazine and OMWCNT–GCE. In order to obtain information on the rate determining step, the anodic Tafel plots were drawn (inset of Fig. 4b). The average of the anodic Tafel slopes of the different plots was obtained as 13.6 V^{-1}. The kinetic parameter of the anodic transfer coefficient, $\alpha_a = 1 - \alpha_c$, is equal $(1-\alpha_c)/0.059$. Thus, the evaluated value for the α_c is 0.2. In addition, the exchange current density, J_0, appears to be readily accessible from the intercept of the Tafel plots and geometric area [39]. The average value of the exchange current density, J_0, for hydrazine oxidation at the modified electrode surface was found to be 0.5 ± 0.01 μA cm^{-2}. The value obtained for J_0 of hydrazine at OMWCNT–GCE is

Table 4 Comparison of the analytical parameters of several modified electrodes for hydrazine determination

Modifier	Method	Linear range (μM)	Sensitivity (μA μM^{-1})	Detection limit (μM)	Reference
Rutin	Amperometry	2.0–190.9	0.0656	0.61	[22]
Caffeic acid	Amperometry	2.5–1,000	3.16	0.40	[23]
Pyrocatechol violet	Amperometry	5.0–500.0	–	4.2	[24]
Hematoxylin	Amperometry	2.0–122.8	0.0208	0.68	[25]
A coumestan derivative	DPV	1.0–40.0	6.1	0.61	[26]
Catechin	Amperometry	2.0–58.4 58.4–237.2	0.0084 0.0052	0.16	[27]
A porphyrin derivative	Amperometry	0.25–250	–	0.03	[51]
An indenedione derivative	DPV	0.6–8.0 8.0–100.0	0.167 0.014	0.29	[52]
An oxadiazole derivative	DPV	0.6–10.0 10.0–400.0	0.0513 0.0107	0.17	This work

higher than the exchange current density at coumestan films (0.4 μA cm^{-2}) [26] but it is lower than the J_0 value of hydrazine at catechin films (0.8 μA cm^{-2}) [27].

Furthermore, chronoamperometry in pH 7.0 phosphate buffer (0.1 M) containing different concentrations of hydrazine was used at OMWCNT−GCE to estimate the diffusion coefficient, D, of hydrazine. Hydrazine diffusion occurs in diffusion layer which located between the electrode surface and the bulk solution. Chronoamperometric data obtained at a potential step of 260 mV are shown in Fig. 5. For an electroactive material with a diffusion coefficient D, the current response under diffusion control was described by Cottrell equation [39]:

$$I = nFAD^{1/2}c\pi^{-1/2}t^{-1/2} \quad (3)$$

Inset A of Fig. 5 shows the experimental plots of I verses $t^{-1/2}$ with the best fit for different concentrations of hydrazine employed. The slopes of the resulting straight line were then plotted versus the hydrazine concentration (inset B of Fig. 5), from which slope we calculated a diffusion coefficient of 6.6×10^{-6} cm^2 s^{-1} for hydrazine.

Table 5 Determination of hydrazine in two water samples using OMWCNT−GCE

Samples	Added (μM)	Found (μM)	RSD (%)	Recovery%
Auxiliary cooling water	–	2.7	2.9	–
	2.5	5.1	3.2	98.1
	5.0	7.9	2.4	102.6
Drinking water	–	>DL	–	–
	20.0	20.6	2.7	103.0
	40.0	40.7	1.8	101.8

Differential pulse voltammetric studies of hydrazine OMWCNT-modified GCE

Differential pulse voltammetry, DPV, has a much higher current sensitivity than cyclic voltammetry, and it can be used to determine the linear range and to estimate the lower limit of hydrazine detection at OMWCNT−GCE. Figure 6 shows the voltammetric response of OMWCNT−GCE to the different hydrazine concentrations. Insets A and B of this figure clearly show that the plot of the peak current versus hydrazine concentration, corrected for any residual current of the modified electrode in supporting electrolyte, is composed of two linear segments with different slopes, corresponding to two different ranges of 0.6–10.0 μM (inset A) and 10.0–400.0 μM (inset B) hydrazine. The decrease of the sensitivity (slope) in the second linear range (Fig. 6, inset B) is likely to be due to the change in catalytic reaction conditions arising from the formation of nitrogen gas bubbles at the surface of OMWCNT−GCE as has been reported elsewhere [32, 33]. In fact, the change in the slopes of the calibration plots arises from the change of the apparent diffusion coefficient of hydrazine, which is smaller when the electrode surface is almost covered by nitrogen bubbles. In other words, the appearance of nitrogen bubbles results rather in lower effective electrode surface. A calibration plot of average differential pulse voltammetric current of three replicate measurements versus hydrazine concentration, in the range of 0.6 to 4.0 μM, was used to estimate the lower detection limit of hydrazine at an OMWCNT−GCE. Having analyzed the data, we estimate that the lower limit of detection of hydrazine is of the order of 0.17 μM according to the definition $Y_{LOD} = Y_B + 3\sigma_B$ [50]. The average voltammetric peak current and the precision estimated in terms of the coefficient of variation for repeated measurements (n=18) of 8.0 μM hydrazine at OMCNT−GCE were 0.41±0.02 μA

and 4.9%, respectively. This coefficient of variation value indicates that OMWCNT−GCE is stable and does not undergo surface fouling during the voltammetric measurements. This also demonstrates the fact that the results obtained at OMWCNT−GCE are repeatable.

In Table 3, some of the analytical characteristics in the present electrochemical technique for hydrazine determination are compared with the value achieved by non-electrochemical techniques. As the results show, some of the values obtained in this work are better than reported for other techniques. The main advantages of the procedure are the enhanced sensitivity, low cost, fairly easy operation, and speed of analysis. Most importantly, identifying the hydrazine oxidation mechanism with other substrates and determination of thermodynamics and kinetic parameters would be made possible via the use of electrochemical methods. In Table 4, some of the response characteristics obtained for hydrazine oxidation on OMWCNT–GCE are compared with those of other modified electrodes and electrochemical techniques applied by other groups [22–27, 51, 52]. As can be seen, the proposed modified electrode is somehow worse in some cases and superior in most others, as compared with the previously reported modified electrodes.

Real samples analysis at OMWCNT−GCE surface

The hydrazine concentration in two aqueous real samples of the auxiliary cooling water, from Yazd Power Generation Management Company (Yazd, Iran), and the drinking water, from Yazd city, were determined on OMWCNT−GCE using the differential pulse voltammetric method. The auxiliary cooling water was diluted five times with 0.1 M phosphate buffer solution (pH=7.0) prior to measurements. Based on the currents of the voltammetric method (n=4) and using the calibration plots which are shown in Fig. 6, insets A and B, the hydrazine concentration in the diluted solution was obtained as 2.7± 0.06 μM. To authenticate the validity of the results, the auxiliary cooling water and the drinking water were spiked with different concentrations of hydrazine. As can be seen in Table 5, the RSD% and recovery rates of the spiked hydrazine were acceptable.

The reliability of the proposed method was also evaluated via comparing the results with those obtained from the standard ASTM method [53] to quantify hydrazine in the same real sample. The total concentration of hydrazine in the cooling water sample was found to be 0.44±0.02 ppm, which is in close agreement with the value of 0.43±0.01 ppm obtained by the present voltammetric method. Based on the t test [54], it can be concluded that there is no evidence of systematic difference between the results obtained by two methods.

Conclusions

In this study, we have demonstrated a new oxadiazole derivative electrodeposited on a MWCNT-modified GCE (OMWCNT−GCE). The redox response of the modified electrode is what was anticipated for a surface-immobilized redox couple. The pH dependence of the redox activity of the oxadiazole is 57.5 mV pH^{-1} unit. This modified electrode exhibits an electrocatalytic behavior to hydrazine oxidation at a much lower overpotential compared with the oxidiazole-modified GCE, MWCNT-modified GCE, and activated GCE. The kinetic parameters, such as the catalytic rate constant, k', the charge transfer coefficient, α, and the exchange current density, J_0, for oxidation of hydrazine at OMWCNT−GCE were determined as $(2.8\pm0.06)\times 10^{-3}$ cm s^{-1}, 0.2 and 0.5 μA cm^{-2}, respectively. The diffusion coefficient of hydrazine was determined as 6.6×10^{-6} cm^2 s^{-1}, using chronoamperometry. The calibration curves for hydrazine determination were obtained in the ranges of 0.6–10.0 μM and 10.0–400.0 μM with differential pulse voltammetry. Finally, OMCNT−GCE has been applied for hydrazine determination in water samples with satisfactory results.

Acknowledgments The authors express their appreciation to the Islamic Azad University (Yazd) Research Council for financial support for this work.

References

1. Majidi MR, Jouyban A, Zeynali KA (2007) Electrochim Acta 52:6248
2. Prabakar SJR, Narayanan SS (2008) J Electroanal Chem 617:111
3. Zheng L, Song JF (2009) Sens Actuators B 135:650
4. Fang B, Zhang C, Zhang W, Wang G (2009) Electrochim Acta 55:178
5. Abbaspour A, Shamsipur M, Siroueinejad A, Kia R, Raithby PR (2009) Electrochim Acta 54:2916
6. Umar A, Rahman MM, Hahn YB (2009) Talanta 77:1376
7. Wang G, Gu A, Wang W, Wei Y, Wu J, Wang G, Zhang X, Fang B (2009) Electrochem Commun 11:631
8. Mo JW, Ogorevc B, Zhang X, Pihlar B (2000) Electroanalysis 12:48
9. Haji Shabani AM, Dadfarnia S, Dehghan K (2004) Bull Korean Chem Soc 25:213
10. Afkhami A, Afshar-E-Asl A (2000) Anal Chim Acta 419:101
11. George M, Nagaraja KS, Balasubramanian N (2008) Talanta 75:27
12. Afkhami A, Zarei AR (2004) Talanta 62:559
13. Safavi A, Karimi MA (2002) Talanta 58:785
14. Safavi A, Baezzat MR (1998) Anal Chim Acta 358:121
15. Yi Q, Yu W (2009) J Electroanal Chem 633:159
16. Karimnezhad G, Jafarloo R, Dorraji PS (2009) Electrochim Acta 54:5721
17. Li J, Lin X (2007) Sens Actuators 126:527
18. Asazawa K, Yamada K, Tanaka H, Taniguchi M, Oguro K (2009) J Power Sources 191:362
19. Zen JM, Kumar AS, Tsai MD (2003) Electroanalysis 15:1073

20. Golabi SM, Zare HR (1999) J Electroanal Chem 465:168
21. Salimi A, Hallaj R (2004) Electroanalysis 16:1964
22. Zare HR, Sobhani Z, Ardakani MM (2007) J Solid State Electrochem 11:971
23. Golabi SM, Zare HR (1999) Electroanalysis 11:1293
24. Golabi SM, Zare HR, Hamzehloo M (2001) Microchem J 69:111
25. Zare HR, Nasirizadeh N (2007) Electrochim Acta 52:4153
26. Zare HR, Nasirizadeh N (2006) Electroanalysis 18:507
27. Zare HR, Habibirad AM (2006) J Solid State Electrochem 10:348
28. Zare HR, Nasirizadeh N (2010) Sens Actuators B 143:666
29. Baughman RH, Zakhidov A, de Heer WA (2002) Science 279:787
30. Ang LM, Hor TSA, Xu GQ, Tung CH, Zhao SP, Wang JLS (2000) Carbon 38:363
31. Che GL, Lakshmi BB, Fisher ER, Martin CR (1998) Nature 393:346
32. Manisankar P, Abirama Sundari PL, Sasikumar R, Palaniappan SP (2008) Talanta 76:1022
33. Yang D, Zhu L, Jiang X (2010) J Electroanal Chem 640:17
34. Salimi A, Hallaj R (2005) Talanta 66:967
35. Moghaddam AB, Ganjali MR, Dinarvand R, Norouzi P, Saboury AA, Moosavi-Movahedi AA (2007) Biophys Chem 128:30
36. Frehill F, Vos JG, Benrezzak S, Koos AA, Konya Z, Ruther MG, Blau WJ, Fonseca A, Nagy JB, Biro LP, Minett AI, Panhuis M (2002) J Am Chem Soc 124:13694
37. Chen RJ, Zhang Y, Wang D, Dai H (2001) J Am Chem Soc 123:3838
38. Fakhari AR, Davarani SSH, Ahmar H, Hasheminasab K, Khavasi HR (2009) J Heterocyclic Chem 46:443
39. Bard AJ, Faulkner LR (2001) Electrochemical methods, fundamentals and applications. Wiley, New York
40. Zare HR, Golabi SM (1999) J Electroanal Chem 464:14
41. Pariente F, Tobalina F, Darder M, Lorenzo E, Abruna HD (1996) Anal Chem 68:3135
42. Jaegfeldt H, Torstensson A, Gorton L, Johansson G (1981) Anal Chem 53:1979
43. Laviron E (1979) J Electroanal Chem 101:19
44. Zare HR, Nasirizadeh N, Ardakani MM (2005) J Electroanal Chem 577:2005
45. Ju H, Shen C (2001) Electroanalysis 13:789
46. Nasirizadeh N, Zare HR (2009) Talanta 80:656
47. Britto PJ, Santhanam KSV, Ajayan PM (1996) Bioelectrochem Bioenerg 41:121
48. Antoniadou S, Jannakoudakis AD, Theodoridou E (1989) Synth Met 30:295
49. Andrieux CP, Saveant JM (1978) J Electroanal Chem 93:163
50. Miller JN, Miller JC (2000) Statistics and chemometrics for analytical chemistry, 4th edn. Pearson Education Ltd., Harlow
51. Quintino MSM, Araki K, Toma HE, Angnes L (2008) Talanta 74:730
52. Zare HR, Nasirizadeh N, Chatraei F, Makarem S (2009) Electrochim Acta 54:2828
53. ASTM D1385−01 Standard test method for hydrazine in water
54. Li X, Zhang S, Sun C (2003) J Electroanal Chem 553:139
55. Chen X, Xiang Y, Li Z, Tong A (2008) Anal Chim Acta 625:41